

# How Much Entanglement Do Quantum Optimization Algorithms Require?

Yanzhu Chen<sup>1</sup>, Linghua Zhu<sup>2</sup>, Chenxu Liu<sup>1</sup>, Nicholas J. Mayhall<sup>3</sup>, Edwin Barnes<sup>1</sup>, and Sophia E. Economou<sup>1</sup>

<sup>1</sup>Department of Physics, Virginia Tech, Blacksburg, VA 24061, U.S.A.

<sup>2</sup>Department of Chemistry, University of Washington, Seattle, WA 98195, U.S.A.

<sup>3</sup>Department of Chemistry, Virginia Tech, Blacksburg, VA 24061, U.S.A.

Many classical optimization problems can be mapped to finding the ground states of diagonal Ising Hamiltonians, for which variational quantum algorithms such as the Quantum Approximate Optimization Algorithm (QAOA) provide heuristic methods. Because the solutions of such classical optimization problems are necessarily product states, it is unclear how entanglement affects their performance. An Adaptive Derivative-Assembled Problem-Tailored (ADAPT) variation of QAOA improves the convergence rate by allowing entangling operations in the mixer layers whereas it requires fewer CNOT gates in the entire circuit. In this work, we study the entanglement generated during the execution of ADAPT-QAOA. Through simulations of the weighted Max-Cut problem, we show that ADAPT-QAOA exhibits substantial flexibility in entangling and disentangling qubits. By incrementally restricting this flexibility, we find that a larger amount of entanglement entropy at earlier stages coincides with faster convergence at later stages. In contrast, while the standard QAOA quickly generates entanglement within a few layers, it cannot remove excess entanglement efficiently. Our results offer implications for favorable features of quantum optimization algorithms.

## 1 Introduction

In today's quantum devices, decoherence sets limits on the circuit depth. Quantum-classical hybrid variational algorithms, which bypass the

need for deep quantum circuits, show promise for providing advantage over purely classical computing [1–5]. In these algorithms, a parametrized ansatz state is realized through a parametrized quantum circuit, on which suitable measurements are carried out to provide information for classical optimization. A suitably chosen ansatz is the key to ensure the correct solution is reached or well approximated. Some approaches, such as the hardware-efficient ansatz, allow the ansatz the capacity of realizing any possible unitary operator in the Hilbert space [6, 7]. On the other hand, a highly expressive ansatz may lead to difficulty in optimization [8–11]. This has prompted a search for more problem-specific algorithms [12–15]. To this end, an Adaptive Derivative-Assembled Problem-Tailored (ADAPT) protocol has been developed [13, 16, 17]. First proposed to find the ground state energies of molecules, the ADAPT protocol constructs the ansatz iteratively, leading to a shallow quantum circuit and fast convergence. Its flexibility also allows one to incorporate some information about the hardware into the ansatz.

The application of hybrid variational algorithms extends beyond simulating physical and chemical systems. In general, optimization problems are of paramount importance to essentially every industry. While it is not yet clear whether quantum computers will offer significant speedups to optimization problems, the huge economic and technological repercussions of such an achievement have motivated the community to explore quantum advantage in the context of optimization. Entanglement has long been considered to play an essential role in quantum computing, although a precise statement in each specific context demands caution [18–20]. The role of entanglement is especially mysterious in quan-

tum optimization algorithms, where both the initial state and the target state are unentangled. Nevertheless, it is often believed that creating some entanglement can provide an advantage to such algorithms. Many classical optimization problems, such as graph coloring and traveling time optimization, can be mapped to finding the ground state of an Ising Hamiltonian, where hybrid variational algorithms can be naturally applied [21–28].

A well-known heuristic algorithm for these problems is the Quantum Approximate Optimization Algorithm (QAOA) [2]. It seeks the solution by optimizing the expectation value of the problem Hamiltonian with respect to an ansatz that alternates between a unitary evolution of the problem Hamiltonian and another unitary that amounts to a simultaneous  $X$  rotation of all the qubits. The generator of the latter is called a mixer operator. Although the ansatz shares similarities with a trotterized version of an adiabatic evolution, its performance is limited by problem features, locality, and symmetry [29–33]. Moreover, analyses of computational resources and experimental requirements for QAOA point out difficulties in its near-term application [34–36].

To improve the performance of QAOA, one can modify it with the ADAPT approach [37, 38]. This algorithm, dubbed ADAPT-QAOA, builds up the ansatz layer by layer. While preserving the alternating structure of QAOA, it replaces the mixer at each step with an operator selected based on the energy gradient. It was observed that convergence was drastically improved in the Max-Cut problem when two-qubit operators were included in the mixer operator pool [37]. Such two-qubit operators provide additional entangling operations in the ansatz. The possibility of having them in the mixer layers lends ADAPT-QAOA more freedom in entanglement production while the standard QAOA can only entangle the qubits through the unitary generated by the Hamiltonian. Despite the fact that ADAPT-QAOA is free to insert more entangling operations in the ansatz, somewhat counterintuitively the final ansatz it produces requires *fewer* CNOT gates overall compared to the standard QAOA for a given convergence threshold [37]. This indicates that the role of entanglement in quantum optimization algorithms is subtle and raises the question of how much entanglement is really needed

to improve convergence.

Depending on the formalism chosen for the computation, entanglement can be seen as the key feature that sets quantum computing apart from classically simulable processes [39, 18]. On the other hand, excessive entanglement in certain settings can make classical optimization harder [40, 41]. Examining entanglement in the context of optimization problems can shed light on the efficiency and favorable features of hybrid variational algorithms. After simulating non-interacting fermions with the hardware efficient ansatz, Ref. [20] concluded that entanglement of an undesirable type can be a hindrance rather than a resource. In the Hamiltonian variational ansatz, entanglement entropy is observed to be between the level required in the ground state and the level in a random state [42]. In classical optimization problems, however, the target states do not intrinsically require a finite amount of entanglement. This makes such problems great testing grounds for studying whether existence of entanglement helps accelerate the optimization process. Ref. [43] suggests that for quadratic unconstrained binary optimization problems a product state ansatz may outperform entangled ones under certain conditions.

In this work, we investigate the role entanglement plays in the performance of ADAPT-QAOA for the weighted Max-Cut problem, which falls in the family of quadratic unconstrained binary optimization problems. We slightly modify the original problem so that the ground state is a product state without any entanglement as opposed to the superposition of the states that differ by flipping all spins. This allows us to remove the entanglement coming from the two-fold degeneracy of the eigenstates. The amount of entanglement entropy at each layer of the algorithm is calculated and compared to that produced by the standard QAOA. From this we find that a larger amount of entanglement entropy does not guarantee a higher convergence rate. Our simulations reveal that ADAPT-QAOA has substantial flexibility in entangling and disentangling qubits. By comparing its performance across different levels of flexibility, we find that a larger amount of entanglement entropy at earlier stages of ADAPT-QAOA can lead to faster convergence at later stages. The rest of the paper is organized as follows. In Sec. 2 we describe the details of our sim-

ulations, with the results summarized in Sec. 3. We conclude and discuss the implications of our work in Sec. 4.

## 2 Numerical simulation

To study the entanglement generated in the process of variational algorithms, we consider the problem of finding the ground state of the Hamiltonian

$$H = \frac{1}{2} \sum_{i < j} w_{ij} (Z_i Z_j - I), \quad (1)$$

where  $\{w_{ij}\}$  are the edge weights of a graph,  $Z_i$  is the Pauli  $Z$  operator acting on the qubit labelled by  $i$ , and  $i, j$  run from 0 to  $n - 1$ . This is equivalent to the weighted Max-Cut problem. All the computational states are eigenstates of  $H$ . Since any two states related by the symmetry  $F = \otimes_i X_i$  share the same energy, there are at least two degenerate ground states. In the standard QAOA, with the reference state, the Hamiltonian, and the mixer operator all respecting the symmetry  $F$ , the solution will always be a symmetric superposition of computational basis states. In ADAPT-QAOA, the selection criterion that determines the mixer operator at each layer ensures that only symmetric operators get selected [37]. Consequently, the solution is also a symmetric superposition. In this work, we focus on the role of entanglement in the performance of the algorithm. To eliminate the effect caused by the entanglement required in the target state, we break the symmetry by adding to  $H$  a small perturbation  $fZ_0$ , where  $f$  is a small positive constant. In this way the ground space degeneracy is lifted, and the target ground state is a unique product state unless an accidental degeneracy is present. Since the identity term in  $H$  only contributes a constant shift to the objective function and a global phase to the ansatz, we drop it and use the cost Hamiltonian

$$\tilde{H} = fZ_0 + \frac{1}{2} \sum_{i < j} w_{ij} Z_i Z_j \quad (2)$$

both as the objective function and in the ansatz.

We simulate the performance of both the standard QAOA and ADAPT-QAOA for 6-vertex degree-5 and 8-vertex degree-7 weighted regular graphs. In each case, 20 instances are generated in which the edge weights are randomly drawn from the discrete set  $\{0.1, 0.2, \dots, 0.8\}$ . We set

$f = 0.05$  so that the symmetry breaking term is always smaller than the energy gaps. To accommodate the symmetry-breaking setting, we choose a symmetry-breaking reference state in ADAPT-QAOA. Specifically, the state of qubit 0 is initialized to  $|1\rangle$  while the other qubits are initially in the state  $|+\rangle$ . The pool  $\mathcal{P}$  from which the mixer operators are selected for ADAPT-QAOA contains more options than the original mixer operator  $M$  for the standard QAOA. For a  $n$ -qubit system, the pool is

$$\begin{aligned} \mathcal{P} = & \left\{ M = \sum_{i=0}^{n-1} X_i, N = \sum_{i=0}^{n-1} Y_i \right\} \\ & \cup \{X_j, Y_j\}_{j=0, \dots, n-1} \\ & \cup \{X_j X_k, Y_j Y_k, X_j Y_k, X_j Z_k, Y_j Z_k\}_{j, k=0, \dots, n-1, j \neq k}. \end{aligned} \quad (3)$$

This is a complete pool, according to Ref. [16], in that the ADAPT-QAOA ansatz built from this pool can approximate any unitary to arbitrary precision given sufficiently many layers. In Ref. [37], a significant improvement in performance is observed for ADAPT-QAOA with this pool compared to standard QAOA. Note that we now restore the operators that anticommute with the operator  $F$  since the symmetry is explicitly broken in our case. At the  $l$ -th layer, the operator  $e^{-i\beta_l A_l} e^{-i\gamma_l \tilde{H}}$  is added to the optimal state at the  $(l - 1)$ -th layer, where the mixer operator  $A_l$  is chosen from  $\mathcal{P}$  after initializing  $\gamma_l$  to some small non-zero value  $\gamma_0$  and  $\beta_l$  to 0 [37]. The selection of the mixer operators takes a greedy approach and follows the ADAPT criterion: Among the operators in the pool, choose the one that maximizes the magnitude of the derivative of the energy (or more generally, the objective function) with respect to the new variational parameter  $\beta_l$  [13, 16, 37]. With the  $l$ -th mixer fixed, *all* the  $2l$  variational parameters in the current ansatz are then (re-)optimized, where the previous  $2(l - 1)$  parameters are initialized to the optimal values obtained in the previous layer. We set the total number of layers to  $p = 10$  for the 6-vertex graphs and to  $p = 14$  for the 8-vertex graphs.

In the standard QAOA, the symmetry-breaking reference state would destroy the similarity to the adiabatic evolution. We include the standard QAOA with both the original reference state and this symmetry-breaking reference state to compare with ADAPT-QAOA.

There have been various strategies for initializing the variational parameters in the standard QAOA [25, 29, 44–46], and an initialization strategy based on optimal parameters for fewer layers has been shown to outperform random initialization [46]. Here, we take an initialization strategy similar to that for ADAPT-QAOA: At the  $l$ -th layer, the  $2(l-1)$  parameters that appear in the  $(l-1)$ -layer ansatz are initialized to the previously optimized values, while the two new parameters in front of  $\tilde{H}$  and  $M$  are initialized to  $\gamma_0$  and 0, respectively.

In summary, the ansätze in ADAPT-QAOA, the standard QAOA, and QAOA with the symmetry breaking reference state are, respectively,

$$|\psi_{A-Q}\rangle = \left( \prod_{l=1}^p e^{-i\beta_l A_l} e^{-i\gamma_l \tilde{H}} \right) |1\rangle_0 \otimes \bigotimes_{i=1}^{n-1} |+\rangle_i, \quad (4)$$

$$|\psi_{QAOA}\rangle = \left( \prod_{l=1}^p e^{-i\beta_l M} e^{-i\gamma_l \tilde{H}} \right) \bigotimes_{i=0}^{n-1} |+\rangle_i, \quad (5)$$

$$|\psi_{QAOAsb}\rangle = \left( \prod_{l=1}^p e^{-i\beta_l M} e^{-i\gamma_l \tilde{H}} \right) |1\rangle_0 \otimes \bigotimes_{i=1}^{n-1} |+\rangle_i. \quad (6)$$

For the optimal state produced at each layer, we calculate the entanglement entropy for two types of bipartitions. One is the entanglement entropy across a middle cut separating half of the qubits from the rest. This measure overlooks the entanglement within either set of qubits, but any possible bias introduced by this particular bipartition will be mitigated after averaging over graphs with randomly generated edge weights. The other is the entanglement entropy between each qubit and the remaining qubits, averaged over all qubits. This measure is 0 if and only if the system is in a product state. By taking the entanglement entropy as the measure, we do not distinguish different entanglement classes [47–51].

In addition to entanglement entropy, we also calculate the entanglement spectrum, which reveals more information about a state [52]. We know that  $\mathcal{P}$  is a complete pool for ADAPT-QAOA, and the controllability of the standard QAOA can be quantified by the dimension of the dynamical Lie algebra generated by  $\tilde{H}$  and  $M$  [53, 46]. With a number of layers that does not grow with the system size, neither ansatz has the capacity to reach all possible states in the Hilbert space. This is a desired feature, since one would

face the challenge of barren plateaus in optimizing a sufficiently generic ansatz [8, 9, 53]. To numerically test how close the distribution of ansatz circuits is to that of random unitaries, we turn to the entanglement spectrum, which has been employed to study the properties of the Hamiltonian variational ansatz [42]. For a state  $|\psi\rangle$  describing a system partitioned into subsystems A and B, it is defined as the spectrum of the operator  $-\log(\rho_A)$ , where

$$\rho_A = \text{Tr}_B(|\psi\rangle\langle\psi|). \quad (7)$$

At each layer, it is calculated for the ansatz state with the variational parameters taking random values. We average over such random parameters and compare it to the entanglement spectrum produced by averaging over random unitary operations that act on the reference state  $\bigotimes_{i=0}^{n-1} |+\rangle_i$ .

### 3 Results

#### 3.1 Comparing ADAPT-QAOA with the standard QAOA

As shown in Fig. 1, with very few layers ADAPT-QAOA finds an entangled optimal state. As the number of layers increases, the entanglement entropy in the solution drops down close to zero as required for the ground state. In contrast, the entanglement entropy of the optimal state found by the standard QAOA increases fast in the first few layers. As the number of layers increases, it remains high, even up to 10 layers. Since ADAPT-QAOA converges more quickly despite generating less entanglement than the standard QAOA, we see that creating more entanglement does not necessarily accelerate the optimization process.

For comparison, in Fig. 2 we include the symmetry-preserving case, in which the  $fZ_0$  term is removed from the cost Hamiltonian both in the ansätze and in the objective function. The symmetric ground state has entanglement entropy  $\log 2$  for both the middle cut and the average 1-qubit cut, which is the maximum amount for the latter. Starting with the same reference state  $\bigotimes_{i=0}^{n-1} |+\rangle_i$ , ADAPT-QAOA produces a larger energy error than the standard QAOA in the first few layers, accompanied by less entanglement entropy for both types of bipartitions. At intermediate stages, the entanglement entropy across

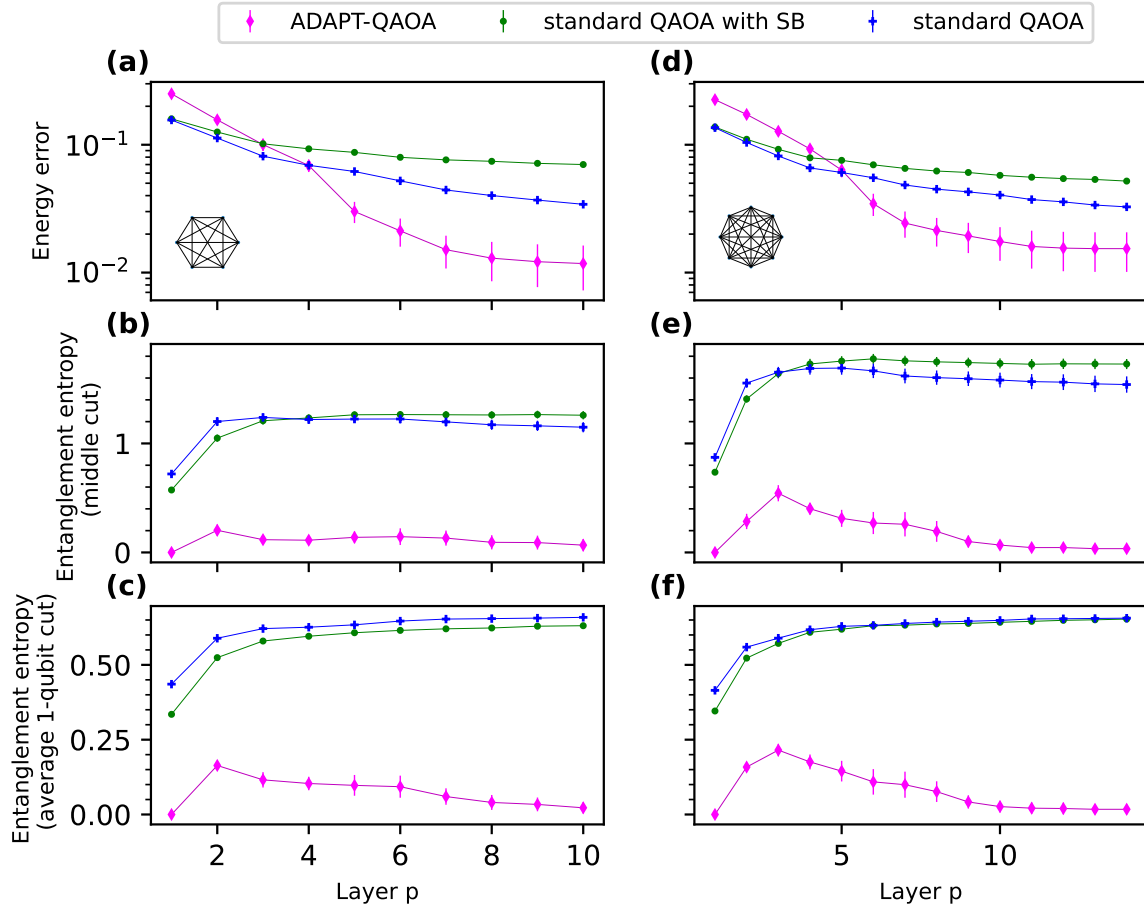


Figure 1: Energy error normalized to the MaxCut value (a, d), entanglement entropy across a middle cut (b, e), and the average entanglement entropy across 1-qubit cuts (c, f) for the optimized state with each given number of QAOA layers, in the symmetry-breaking case. The panels on the left (a, b, c) and right (d, e, f) are for the 6-qubit and 8-qubit regular graphs, respectively. The performance of ADAPT-QAOA (magenta diamond) is compared to that generated by the standard QAOA with a symmetry-breaking reference state (green dot) or with a symmetric reference state (blue cross). The error bars show the error in the mean.

the middle cut generated by ADAPT-QAOA gets close to or exceeds that generated by the standard QAOA. As the number of layers further increases, it drops fast towards the target level while that generated by the standard QAOA changes little in subsequent layers. For the entanglement entropy across the average 1-qubit cut, the amount generated by ADAPT-QAOA keeps rising at a roughly constant rate until it reaches the target level. In contrast, the amount generated by the standard QAOA rises fast in the first few layers but drastically slows down at later stages.

In Fig. 2, we also show the remaining entanglement entropy of the state after projecting one arbitrary qubit onto the state  $|0\rangle$ . At any layer, the ansatz state is a symmetric superposition of states, but the projection selects one component

out of any pair of states related by the spin flip  $F$ . In this way, the symmetric ground state will be projected to a product state whose entanglement entropy is 0. Similar to the symmetry-breaking case, we observe at early stages a rapid increase and at late stages a slow decrease of entanglement entropy for the standard QAOA compared to ADAPT-QAOA.

The symmetry-breaking and the symmetry-preserving cases together demonstrate that the additional flexibility in ADAPT-QAOA allows it to control the rise and fall of entanglement to its advantage. With few layers, both algorithms are capable of finding solutions with more entanglement than required. With more layers, however, ADAPT-QAOA can remove the excess entanglement far more efficiently than the standard

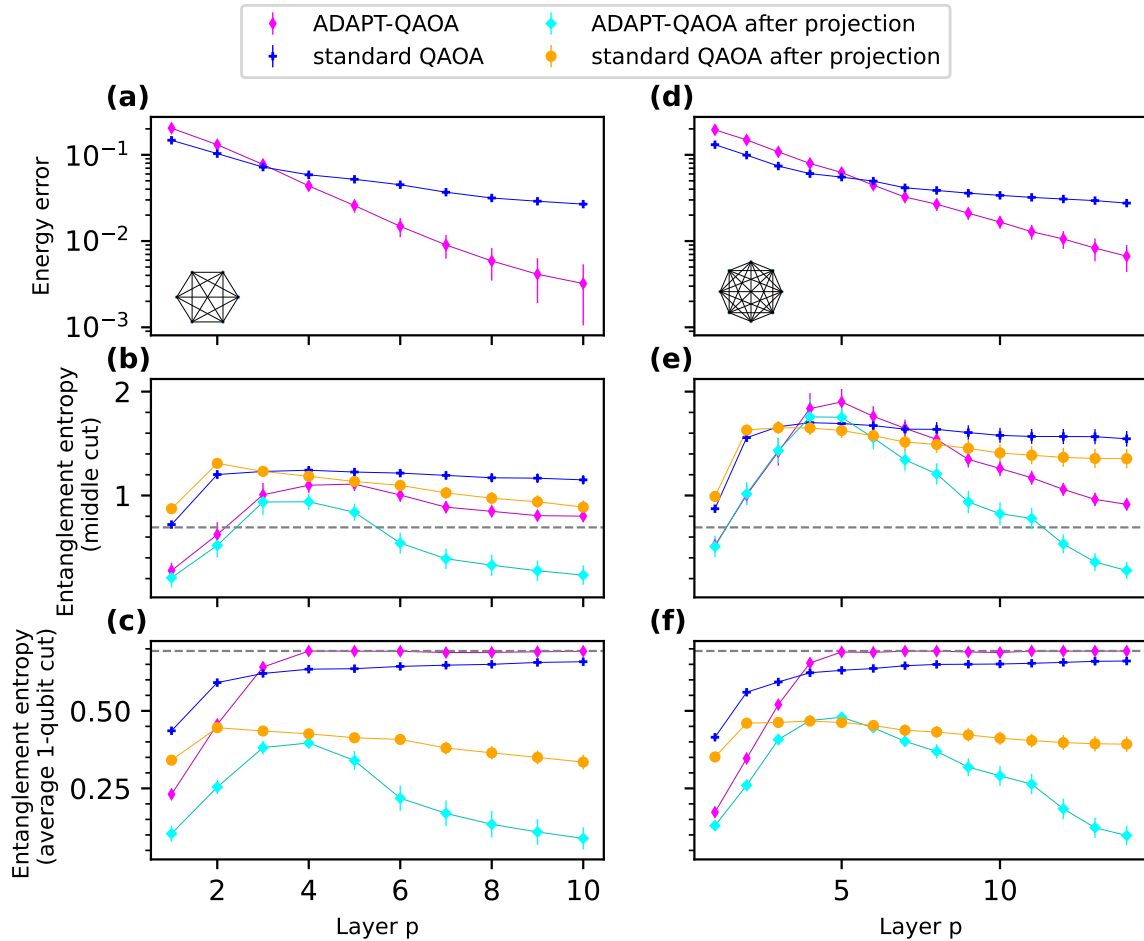


Figure 2: Energy error normalized to the MaxCut value (a, d), entanglement entropy across a middle cut (b, e), and the average entanglement entropy across 1-qubit cuts (c, f) for the optimized state with each given number of QAOA layers, in the symmetry-preserving case. The panels on the left (a, b, c) and right (e, f, g) are for the 6-qubit and 8-qubit regular graphs, respectively. The performance of ADAPT-QAOA (magenta diamond) is compared to that generated by the standard QAOA (blue cross). The grey dashed horizontal lines in (b, c, e, f) are the entanglement entropies of the symmetric ground state. The entanglement entropy after projection is plotted for ADAPT-QAOA (big cyan diamond) and the standard QAOA (big orange dot) and the entanglement entropy across a middle cut is normalized in this case. The error bars show the error in the mean.

QAOA. We attribute this to the two-qubit mixer operators in the ADAPT-QAOA ansatz. Their presence helps with both the production and the removal of entanglement in the state whereas the Hamiltonian is the only operation in the standard QAOA ansatz that can do so.

Due to this flexibility, ADAPT-QAOA can reach the same energy accuracy with fewer layers than the standard QAOA, bringing down the total number of entangling gates in the circuit. Fig. 3 shows the number of CNOT gates and the number of variational parameters required in the ansatz circuit when the energy error gets below the threshold 0.04. Although the mixer operators in the ADAPT-QAOA ansatz introduce

additional CNOT gates, the dominant source of CNOT gates is the cost Hamiltonian, and overall ADAPT-QAOA is more economical in entangling operations. For some of the 20 graph instances, the energy error has not reached the threshold at the last layer, in which case we set the number of CNOT gates and the number of parameters as the maximum values in the 10-layer (14-layer) ansatz for the 6-qubit (8-qubit) graphs. This underestimates these counts. We remark that the undercounting has the most impact on the standard QAOA with the symmetry-breaking reference state, where both of the counts are much higher than in the other two cases. ADAPT-QAOA and the standard QAOA are affected sim-

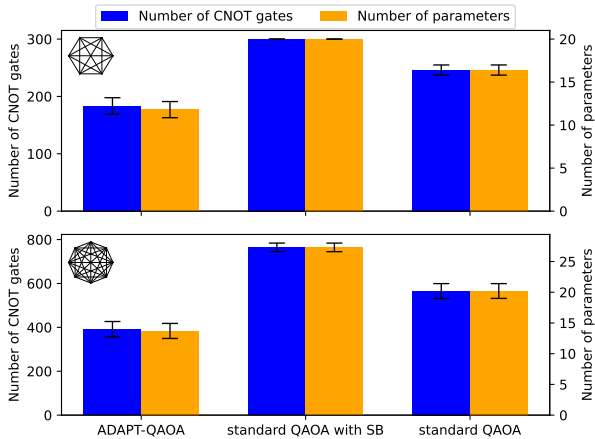


Figure 3: Number of CNOT gates (left, blue) and number of variational parameters (right, orange) required by ADAPT-QAOA, the standard QAOA with a symmetry-breaking reference state, and the standard QAOA with a symmetric reference state, when the energy error normalized to the MaxCut value reaches the threshold 0.04 in the symmetry-breaking case. The error bars show the error in the mean. Panels (a) and (b) are for the 6-qubit and 8-qubit regular graphs, respectively. The numbers are undercounted due to the cutoff at 10 (14) layers for the 6-qubit (8-qubit) graphs.

ilarly, with close numbers of instances suffering undercounting.

### 3.2 Comparing different levels of flexibility in ADAPT-QAOA

The observation that ADAPT-QAOA is able to generate an appropriate amount of entanglement can be reinforced by examining its performance as we constrain its flexibility to varying degrees. If a quantum device has limited connectivity, it is costly to realize an entangling gate between the qubits that are not directly connected. This is common in quantum processors such as superconducting devices. One can adjust the mixer operator pool accordingly, for example, by limiting the two-qubit operators to those supported on directly connected pairs. With fewer options for entangling operations, we expect ADAPT-QAOA to show slower convergence when averaging over graphs with different edge weights. This is confirmed by simulation, where we take two configurations with the 6 qubits arranged on a  $2 \times 3$  grid and a line, respectively. The only two-qubit operators in the pool are those on the nearest-neighbor qubits.

One feature accompanying slower convergence

is less efficient entanglement generation, as shown in Fig. 4. In the first few layers the ADAPT-QAOA ansatz cannot reach the target state yet even with a fully-connected pool. At this stage, the energy expectation values of the optimal states are close to each other regardless of the operator pool. Despite similar energies, ADAPT-QAOA with full connectivity produces more entanglement entropy than with reduced connectivity. With more layers, it is able to disentangle more quickly and get close to the target state whereas reduced connectivity leads to a solution with more entanglement entropy than needed. In this case, better overall performance coincides with more entanglement entropy at earlier stages of the algorithm, an indication that more entanglement than required in the target state can be helpful.

### 3.3 Entanglement spectrum

With the ability to take any operators from the pool  $\mathcal{P}$ , ADAPT-QAOA can in principle generate all possible unitaries if there are no restrictions on the number of layers. For each problem, the operator selection process ensures that the ansatz is specific. As the number of layers increases, the ansatz becomes more expressive. We compare the ansatze produced at each layer by ADAPT-QAOA, the standard QAOA with the symmetry-breaking reference state, and the standard QAOA. In each case, we replace the optimized variational parameters in the ansatz with values randomly drawn from  $[0, 20\pi)$ , and average over 1000 such states for the ansatz associated with one graph instance. This offers an indirect probe into how general the possible states for a chosen ansatz can be.

In Fig. 5, we present the entanglement spectrum across a middle cut given each number of layers, averaged over the 20 graph instances. Qualitatively, the entanglement spectrum becomes more similar to that produced by random unitaries as the number of layers increases for both ADAPT-QAOA and the standard QAOA. Interestingly, in terms of the average entanglement spectrum produced, the standard QAOA ansatz approaches the random unitary quickly. With the symmetry-breaking reference state, it takes more layers than with the symmetric reference state. With both reference states, however, the standard QAOA ansatz approaches the ran-

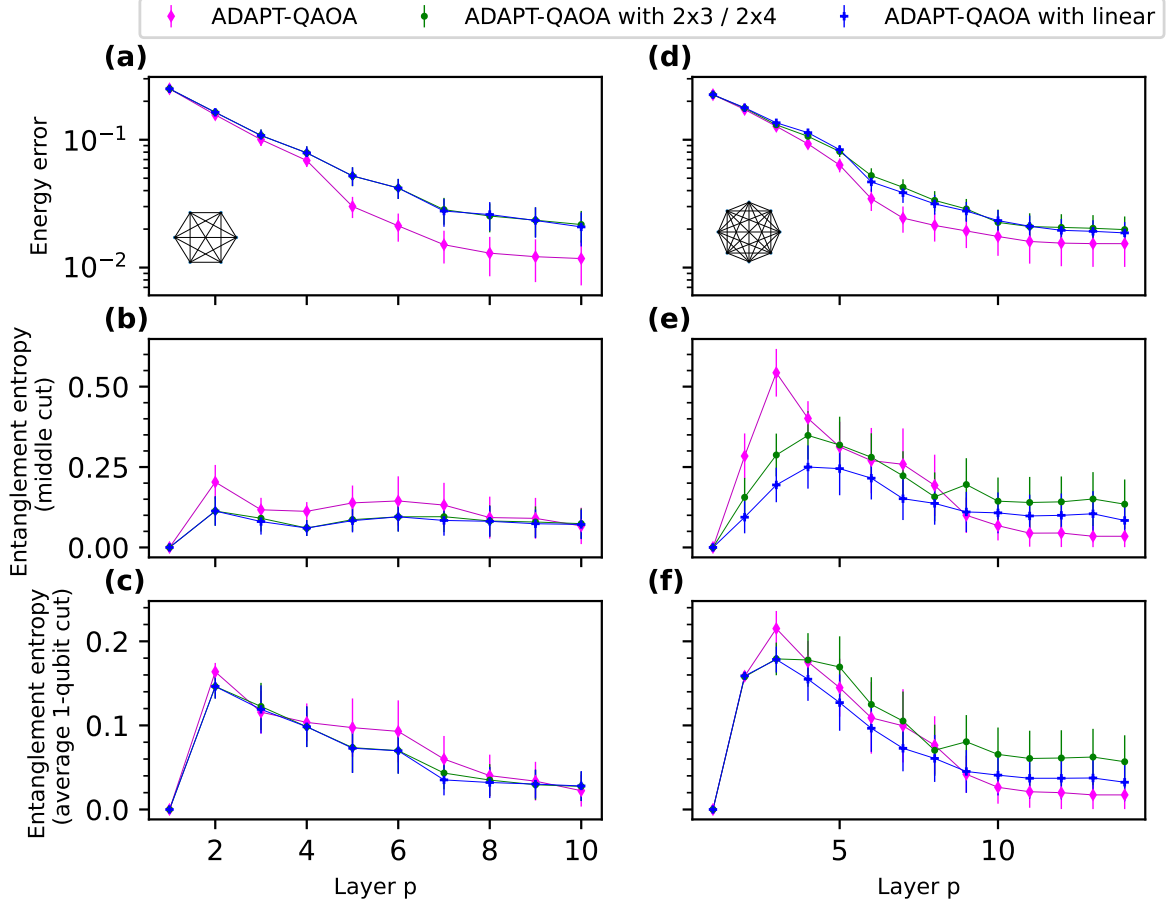


Figure 4: Energy error normalized to the MaxCut value (a, d), entanglement entropy across a middle cut (b, e), and the average entanglement entropy across 1-qubit cuts (c, f) for the optimized state with each given number of QAOA layers. The entanglement entropy generated by ADAPT-QAOA with full connectivity (magenta diamond) is compared to that generated by ADAPT-QAOA whose potential mixer operators are restricted to the nearest neighbors on a  $2 \times 3$  (in the 6-qubit case) or  $2 \times 4$  (in the 8-qubit case) configuration (green dot) or a linear configuration (blue cross). The error bars show the error in the mean.

dom unitary faster than ADAPT-QAOA. This suggests that the ADAPT-QAOA ansatz is less generic, leading to easier optimization of the variational parameters.

As is seen above, the average entanglement spectrum in possible ansatz states is sensitive to the reference state. We repeat this simulation for the symmetry-preserving case without the  $fZ_0$  term, in which case the reference state is  $\bigotimes_{i=0}^{n-1} |+\rangle_i$  for both ADAPT-QAOA and the standard QAOA. The result is plotted in Fig. 6. We find that in this case ADAPT-QAOA also needs more layers to approach the random unitary than the standard QAOA.

## 4 Conclusion and discussion

In this work we investigate the role of entanglement in solving MaxCut problems with quantum optimization algorithms, where a finite amount of entanglement is not required in the target state. In the context of QAOA and its adaptive variation ADAPT-QAOA, we find that the algorithm performance can benefit from entanglement generation in the process. On the other hand, the relation between the convergence speed and the amount of entanglement in the intermediate state is not a simple positive correlation and it can be counterproductive to create too much entanglement.

In particular, by comparing the entanglement generated by ADAPT-QAOA at various stages of

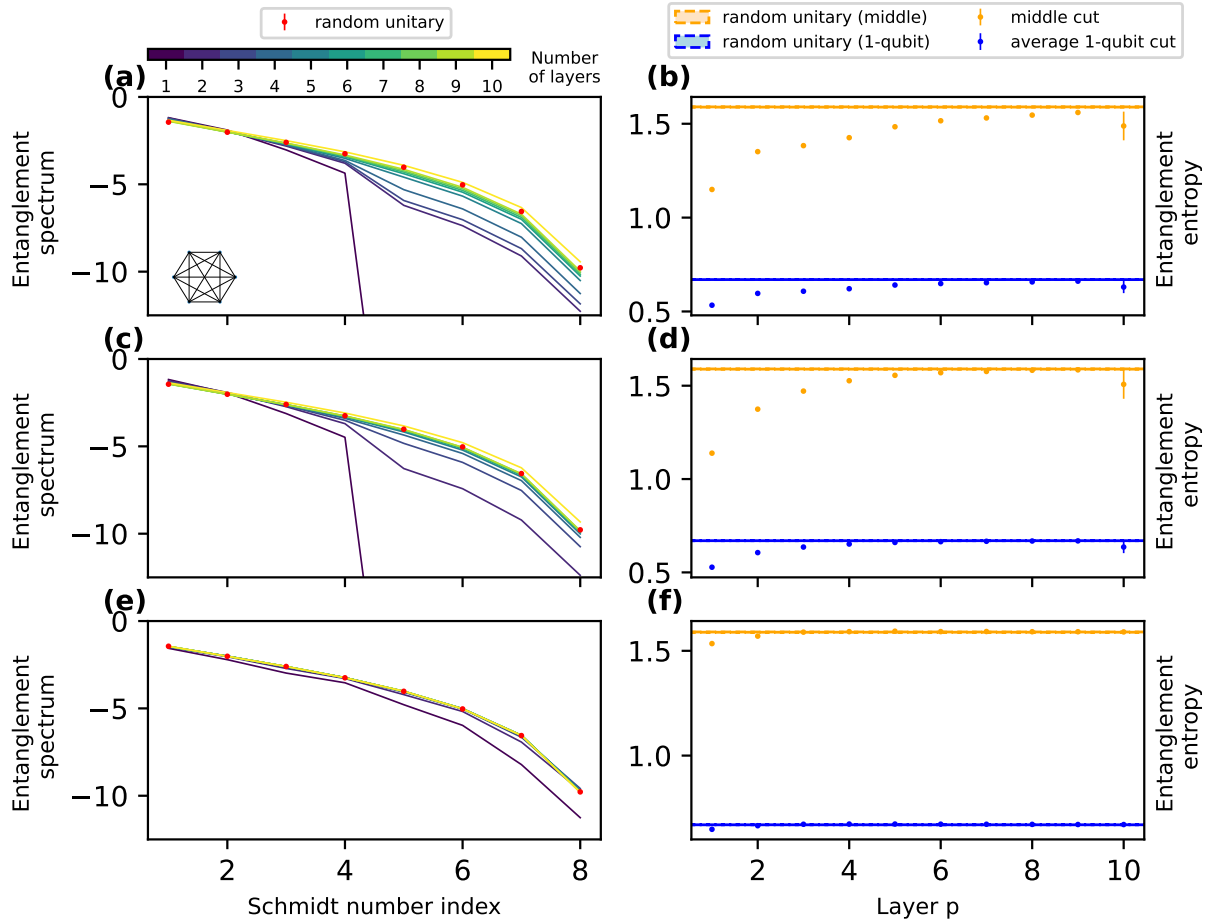


Figure 5: Entanglement spectrum, entanglement entropy across a middle cut, and the average entanglement entropy across 1-qubit cuts for the ADAPT-QAOA ansatz (a, b), the standard QAOA ansatz with a symmetry-breaking reference state (c, d), and the standard QAOA ansatz (e, f), respectively, with the variational parameters randomly sampled between 0 and  $20\pi$ . We average over the ansatzes produced for the previously sampled edge weight sets. The error bars show the error in the mean. The values cut off at the bottom of the graph approach negative infinity.

the algorithm to that generated by the standard QAOA, we observe that although the standard QAOA can quickly generate more entanglement entropy with only a few layers in the ansatz, it is inefficient in removing excess entanglement as the number of layers increases. Consequently, at later stages it does not perform as well as ADAPT-QAOA, in which both the Hamiltonian and the selected two-qubit mixer operators contribute to entanglement generation and removal. The larger amount of entanglement entropy at earlier stages does not imply faster convergence in the entire process. We then restrict the flexibility of ADAPT-QAOA to see if more excess entanglement implies slower convergence in our classical optimization setting. We find that the version with the largest degree of flexibility produces more entanglement entropy at earlier stages and

converges faster at later stages. Finally, the average entanglement spectrum of the possible states for each ansatz suggests that with a given number of layers, ADAPT-QAOA is less expressive than the standard QAOA, which can reduce the difficulty in the classical optimization component of the variational algorithm.

These observations provide qualitative guidance in designing quantum optimization algorithms. Specifically, variational algorithms equipped with flexibility in entangling operations can outperform the algorithms with limited entangling operations. From this perspective, ADAPT-QAOA and the ADAPT approach in general demonstrate great potential in generating a suitable amount of entanglement for the optimization task. To offer better flexibility, the mixer operator pool should include multi-

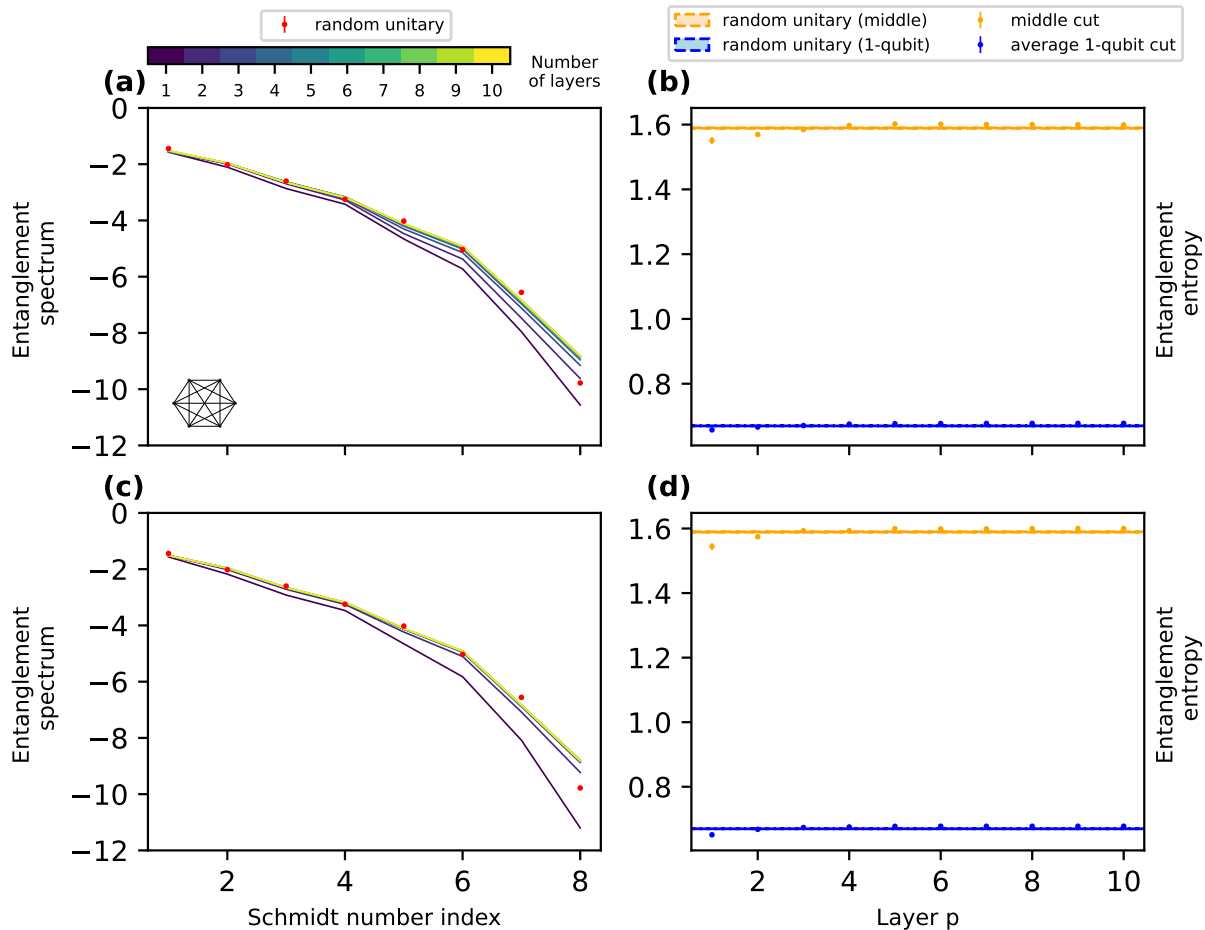


Figure 6: Entanglement spectrum, entanglement entropy across a middle cut, and the average entanglement entropy across 1-qubit cuts for the ADAPT-QAOA ansatz (a, b) and the standard QAOA ansatz (c, d), respectively, with the variational parameters randomly sampled between 0 and  $20\pi$  in the symmetry-preserving case. We average over the ansatzes produced for the previously sampled edge weight sets. The error bars show the error in the mean.

qubit operators beyond those supported on nearest neighbors. It will thus be easier to demonstrate ADAPT-QAOA on platforms with less limitation on entangling operations between arbitrary pairs of qubits, such as trapped ion systems [54–56] and Rydberg atoms [57–59].

In our work, entanglement is quantified by the entanglement entropy associated with a bipartition, which does not reveal the many-body structure of the entanglement. Multipartite entanglement, where the number of parties grows with the system size, is necessary if the quantum algorithm is exponentially hard to simulate classically [18]. It thus remains to be investigated whether the heuristic quantum optimization algorithms studied here offer any advantage, exponential or polynomial, over classical algorithms.

## Acknowledgements

S. E. E. acknowledges support from the US Department of Energy (Award No. DE-SC0019318). E.B. and N.J.M. acknowledge support from the US Department of Energy (Award No. DE-SC0019199).

## References

- [1] A. Peruzzo, J. McClean, P. Shadbolt, M.-H. Yung, X.-Q. Zhou, P. J. Love, A. Aspuru-Guzik, and J. L. O’Brien, *Nat. Phys.* **5**, 4213 (2014).
- [2] E. Farhi, J. Goldstone, and S. Gutmann, [arXiv:1411.4028](https://arxiv.org/abs/1411.4028) (2014), 10.48550/arxiv.1411.4028.
- [3] E. Farhi and A. W. Har-

- row, [arXiv:1602.07674](https://arxiv.org/abs/1602.07674) (2016), [10.48550/ARXIV.1602.07674](https://arxiv.org/abs/1602.07674).
- [4] J. R. McClean, J. Romero, R. Babbush, and A. Aspuru-Guzik, *New J. Phys.* **18**, 023023 (2016).
- [5] M. Cerezo, A. Arrasmith, and e. a. Ryan Babbush, *Nat. Rev. Phys.* **3**, 625–644 (2021).
- [6] A. Kandala, A. Mezzacapo, K. Temme, M. Takita, M. Brink, J. M. Chow, and J. M. Gambetta, *Nature* **549**, 242 (2017).
- [7] S. Sim, P. Johnson, and A. Aspuru-Guzik, *Adv. Quantum Technol.* **2**, 1900070 (2019).
- [8] J. R. McClean, S. Boixo, V. N. Smelyanskiy, R. Babbush, and H. Neven, *Nat. Commun.* **9**, 4812 (2018).
- [9] M. Cerezo, A. Sone, T. Volkoff, L. Cincio, and P. J. Coles, *Nat. Commun.* **12**, 1791 (2021).
- [10] A. Arrasmith, Z. Holmes, M. Cerezo, and P. J. Coles, “Equivalence of quantum barren plateaus to cost concentration and narrow gorges,” (2021).
- [11] Z. Holmes, K. Sharma, M. Cerezo, and P. J. Coles, *PRX Quantum* **3**, 010313 (2022).
- [12] D. Wecker, M. B. Hastings, and M. Troyer, *Phys. Rev. A* **92**, 042303 (2015).
- [13] H. R. Grimsley, E. Barnes, S. E. Economou, and N. J. Mayhall, *Nat. Commun.* **10**, 3007 (2019).
- [14] S. Hadfield, Z. Wang, B. O’Gorman, E. G. Rieffel, D. Venturelli, and R. Biswas, *Algorithms* **12** (2019), [10.3390/a12020034](https://arxiv.org/abs/10.3390/a12020034).
- [15] A. Choquette, A. Di Paolo, P. K. Barkoutsos, D. Sénéchal, I. Tavernelli, and A. Blais, *Phys. Rev. Research* **3**, 023092 (2021).
- [16] H. L. Tang, V. Shkolnikov, G. S. Barron, H. R. Grimsley, N. J. Mayhall, E. Barnes, and S. E. Economou, *PRX Quantum* **2**, 020310 (2021).
- [17] V. O. Shkolnikov, N. J. Mayhall, S. E. Economou, and E. Barnes, [arXiv:2109.05340](https://arxiv.org/abs/2109.05340) (2021), [10.48550/ARXIV.2109.05340](https://arxiv.org/abs/10.48550/ARXIV.2109.05340).
- [18] R. Jozsa and N. Linden, *Proc. R. Soc. Lond. A* **459**, 2011–2032 (2003).
- [19] D. Gross, S. T. Flammia, and J. Eisert, *Phys. Rev. Lett.* **102**, 190501 (2009).
- [20] A. J. C. Woitzik, P. K. Barkoutsos, F. Wudarski, A. Buchleitner, and I. Tavernelli, *Phys. Rev. A* **102**, 042402 (2020).
- [21] A. Lucas, *Frontiers in Physics* **2**, 5 (2014).
- [22] G. Kochenberger, J.-K. Hao, F. Glover, M. Lewis, Z. Lü, H. Wang, and Y. Wang, *J. Comb. Optim.* **28**, 58 (2014).
- [23] S. Hadfield, Z. Wang, E. G. Rieffel, B. O’Gorman, D. Venturelli, and R. Biswas, in *Proceedings of the Second International Workshop on Post Moores Era Supercomputing*, PMES’17 (Association for Computing Machinery, New York, NY, USA, 2017) p. 15–21.
- [24] Y.-H. Oh, H. Mohammadbagherpoor, P. Dreher, A. Singh, X. Yu, and A. J. Rindos, [arXiv:1911.00595](https://arxiv.org/abs/1911.00595) (2019), [10.48550/ARXIV.1911.00595](https://arxiv.org/abs/10.48550/ARXIV.1911.00595).
- [25] R. Shaydulin, I. Safro, and J. Larson, in *2019 IEEE High Performance Extreme Computing Conference (HPEC)* (2019) pp. 1–8.
- [26] Z. Tabi, K. H. El-Safty, Z. Kallus, P. Hága, T. Kozsik, A. Glos, and Z. Zimborás, in *2020 IEEE International Conference on Quantum Computing and Engineering (QCE)* (2020) pp. 56–62.
- [27] S. Bravyi, A. Kliesch, R. Koenig, and E. Tang, *Quantum* **6**, 678 (2022).
- [28] J. R. Weggemans, A. Urech, A. Rausch, R. Spreeuw, R. Boucherie, F. Schreck, K. Schoutens, J. Minář, and F. Speelman, *Quantum* **6**, 687 (2022).
- [29] L. Zhou, S.-T. Wang, S. Choi, H. Pichler, and M. D. Lukin, *Phys. Rev. X* **10**, 021067 (2020).
- [30] V. Akshay, H. Philathong, M. E. S. Morales, and J. D. Biamonte, *Phys. Rev. Lett.* **124**, 090504 (2020).
- [31] S. Bravyi, A. Kliesch, R. Koenig, and E. Tang, *Phys. Rev. Lett.* **125**, 260505 (2020).
- [32] E. Farhi, D. Gamarnik, and S. Gutmann, [arXiv:2004.09002](https://arxiv.org/abs/2004.09002) (2020), [10.48550/ARXIV.2004.09002](https://arxiv.org/abs/10.48550/ARXIV.2004.09002).
- [33] E. Farhi, D. Gamarnik, and S. Gutmann, [arXiv:2005.08747](https://arxiv.org/abs/2005.08747) (2020), [10.48550/ARXIV.2005.08747](https://arxiv.org/abs/10.48550/ARXIV.2005.08747).
- [34] G. G. Guerreschi and A. Y. Matsuura, *Sci. Rep.* **9**, 6903 (2019).
- [35] M. P. Harrigan, K. J. Sung, and e. a. Matthew Neeley, *Nat. Phys.* **17**, 332 (2021).
- [36] J. Weidenfeller, L. C. Valor, J. Gacon, C. Tornow, L. Bello, S. Woerner, and

- D. J. Egger, [arXiv:2202.03459](#) (2022), [10.48550/ARXIV.2202.03459](#).
- [37] L. Zhu, H. L. Tang, G. S. Barron, F. A. Calderon-Vargas, N. J. Mayhall, E. Barnes, and S. E. Economou, [arXiv:2005.10258](#) (2020), [10.48550/ARXIV.2005.10258](#).
- [38] A. Warren, L. Zhu, N. J. Mayhall, E. Barnes, and S. E. Economou, [arXiv:2203.12757](#) (2022), [10.48550/ARXIV.2203.12757](#).
- [39] A. Ekert and R. Jozsa, *Phil. Trans. R. Soc. A.* **356**, 1769–1782 (1998).
- [40] T. L. Patti, K. Najafi, X. Gao, and S. F. Yelin, *Phys. Rev. Research* **3**, 033090 (2021).
- [41] C. Ortiz Marrero, M. Kieferová, and N. Wiebe, *PRX Quantum* **2**, 040316 (2021).
- [42] R. Wiersema, C. Zhou, Y. de Sereville, J. F. Carrasquilla, Y. B. Kim, and H. Yuen, *PRX Quantum* **1**, 020319 (2020).
- [43] P. Díez-Valle, D. Porras, and J. J. García-Ripoll, *Phys. Rev. A* **104**, 062426 (2021).
- [44] S. H. Sack and M. Serbyn, *Quantum* **5**, 491 (2021).
- [45] J. Li, M. Alam, and S. Ghosh, [arXiv:2102.13288](#) (2021), [10.48550/ARXIV.2102.13288](#).
- [46] B. Zhang, A. Sone, and Q. Zhuang, [arXiv:2109.13346](#) (2021), [10.48550/ARXIV.2109.13346](#).
- [47] V. Coffman, J. Kundu, and W. K. Wootters, *Phys. Rev. A* **61**, 052306 (2000).
- [48] T.-C. Wei and P. M. Goldbart, *Phys. Rev. A* **68**, 042307 (2003).
- [49] S. Virmani, M. Sacchi, M. Plenio, and D. Markham, *Physics Letters A* **288**, 62 (2001).
- [50] M. B. Plenio and S. Virmani, *Quantum Inf. Comput.* **7**, 1 (2007).
- [51] R. Horodecki, P. Horodecki, M. Horodecki, and K. Horodecki, *Rev. Mod. Phys.* **81**, 865 (2009).
- [52] H. Li and F. D. M. Haldane, *Phys. Rev. Lett.* **101**, 010504 (2008).
- [53] M. Larocca, P. Czarnik, K. Sharma, G. Muraleedharan, P. J. Coles, and M. Cerezo, [arXiv:2105.14377](#) (2021), [10.48550/ARXIV.2105.14377](#).
- [54] K. A. Landsman, Y. Wu, P. H. Leung, D. Zhu, N. M. Linke, K. R. Brown, L. Duan, and C. Monroe, *Phys. Rev. A* **100**, 022332 (2019).
- [55] C. Zhang, F. Pokorny, W. Li, G. Higgins, A. Pöschl, I. Lesanovsky, and M. Hennrich, *Nature* **580**, 345 (2020).
- [56] R. Blümel, N. Grzesiak, N. Pimenti, K. Wright, and Y. Nam, *npj Quantum Inf* **7**, 147 (2021).
- [57] H. Levine, A. Keesling, G. Semeghini, *et al.*, *Phys. Rev. Lett.* **123**, 170503 (2019).
- [58] T. M. Graham, M. Kwon, B. Grinkemeyer, Z. Marra, X. Jiang, M. T. Lichtman, Y. Sun, M. Ebert, and M. Saffman, *Phys. Rev. Lett.* **123**, 230501 (2019).
- [59] T. Graham, Y. Song, J. Scott, *et al.*, *Nature* **604**, 457 (2022).